AGU ADVANCING EARTH AND SPACE SCIENCES

Geophysical Research Letters

RESEARCH LETTER
10.1029/2024GL112717

Climate-Dependency of Impact of Increased Carbon Dioxide on African Monsoon Rainfall: Insights From Model Simulations

Xiaoxu Shi[1,2], Martin Werner[2], Francesco S. R. Pausata[3], Jiping Liu[1,4], Roberta D'Agostino[5], Yongyun Hu[6], Hu Yang[1], Hang Wang[1,4], Chaoyuan Yang[1], and Gerrit Lohmann[2]

[1]Southern Marine Science and Engineering Guangdong Laboratory (Zhuhai), Zhuhai, China, [2]Alfred Wegener Institute, Helmholtz Center for Polar and Marine Research, Bremerhaven, Germany, [3]University of Quebec in Montreal, Montreal, QC, Canada, [4]School of Atmospheric Sciences, Sun Yat-sen University, Zhuhai, China, [5]Italian National Research Council, Institute of Atmospheric Sciences and Climate, Lecce, Italy, [6]Peking University, Peking, China

Key Points:

- The impact of rising CO_2 on African summer monsoon rainfall is climate dependent
- Under interglacial climate background, a rise in CO_2 can enhance northern Africa precipitation by increasing atmospheric moisture content
- In glacial times, a rise in CO_2 facilitates a dryness over most northern Africa, primarily due to a weakened tropical circulation

Supporting Information:

Supporting Information may be found in the online version of this article.

Correspondence to:

X. Shi and J. Liu,
shixiaoxu@sml-zhuhai.cn;
liujp63@mail.sysu.edu.cn

Citation:

Shi, X., Werner, M., Pausata, F. S. R., Liu, J., D'Agostino, R., Hu, Y., et al. (2025). Climate-dependency of impact of increased carbon dioxide on African monsoon rainfall: Insights from model simulations. *Geophysical Research Letters*, *52*, e2024GL112717. https://doi.org/10.1029/2024GL112717

Received 27 SEP 2024
Accepted 27 MAR 2025

Author Contributions:

Conceptualization: Xiaoxu Shi
Data curation: Xiaoxu Shi
Formal analysis: Xiaoxu Shi
Methodology: Xiaoxu Shi, Martin Werner, Francesco S. R. Pausata, Jiping Liu
Project administration: Gerrit Lohmann
Supervision: Martin Werner, Jiping Liu
Visualization: Xiaoxu Shi
Writing – original draft: Xiaoxu Shi
Writing – review & editing: Xiaoxu Shi, Martin Werner, Francesco S. R. Pausata, Jiping Liu, Roberta D'Agostino, Yongyun Hu, Hu Yang, Hang Wang, Chaoyuan Yang, Gerrit Lohmann

Abstract

Previous studies on future scenarios identified two key effects of increasing CO_2 on the African summer monsoon (ASM): Rising CO_2 leads to an enhancement in moisture supply, favoring an increase in ASM precipitation (the thermodynamic effect). However, it also results in a weakening in mean atmospheric flow, thus facilitating a dryness across the ASM region (the dynamic effect). Therefore, the ultimate change in ASM precipitation stems from the balance of both the thermodynamic and dynamic effects. This study further examines the impact of rising CO_2 on ASM rainfall, by taking into account various climate states. Our results suggest that an increase in CO_2 during warm interglacial periods has a stronger influence from thermodynamic factors than from dynamic factors, resulting in an enhancement in ASM rainfall. In contrast, if CO_2 increases under cold glacial climate backgrounds, its dynamic impact dominates a reduction of rainfall in most ASM region.

Plain Language Summary

The increase in carbon dioxide (CO_2) levels influences African monsoon rainfall mainly via two processes. First, the warming induced by rising CO_2 leads to enhanced evaporation, thereby increasing atmospheric water vapor content, which provides a greater moisture supply for precipitation formation (the "thermodynamic effect"). Second, rising CO_2 also weakens the tropical circulation, which influences the dynamics of monsoon rainfall (the "dynamic effect"). Consequently, the final changes in monsoon rainfall are determined by the combined effects of these two processes. In this study, through a set of sensitivity simulations, we investigated the impact of rising CO_2 on African summer monsoon (ASM) rainfall during different climatic periods. Although the response in monsoon precipitation is not spatially uniform, our results generally indicate that increased CO_2 levels exert a greater thermodynamic impact than a dynamic one during relatively warm interglacial periods, resulting in strengthened monsoon rainfall. Conversely, a dryness over most of the ASM region is dominated by the dynamic effect when CO_2 increases during cool glacial periods. This research contributes to our understanding of the complex interplay between CO_2 levels, thermodynamic processes, and dynamic processes in shaping African summer monsoon rainfall. It also underscores the importance of considering climatic periods and the relative strengths of different mechanisms when assessing the impact of CO_2 on monsoon systems.

1. Introduction

The African Summer Monsoon (ASM) is a key component of global monsoon systems. The rainfall associated with the ASM bears high socio-economic importance (Odoulami & Akinsanola, 2018). Hence, it is essential to improve our understanding of the potential changes in African precipitation patterns due to climate changes. However, the impact of global warming on ASM rainfall is complicated by significant heterogeneity among models (Biasutti, 2013; Dosio et al., 2021; Dosio & Panitz, 2016; Laprise et al., 2013; Rowell et al., 2016). Some studies indicate that an increase in carbon dioxide (CO_2) concentrations is likely to intensify African monsoon rainfall (e.g., Akinsanola & Zhou, 2019b; Akinsanola et al., 2020; Gaetani et al., 2017; Gbode et al., 2021; He et al., 2020; James & Washington, 2013; Maynard et al., 2002). For example, under the Representative Concentration Pathway global warming scenarios RCP4.5 and RCP8.5, precipitation is projected to increase in most parts of northern Africa (Akinsanola & Zhou, 2019b; Akinsanola et al., 2020). The results of a 150-year transient climate simulation for 1950–2100, which accounts for a gradual increase of CO_2, predict a notable increase in monsoon precipitation in West Africa by the end of the 21st century (Maynard et al., 2002). Simulation results based on the Climate Earth System Model (CESM) also project a substantial increase in rainfall in West Africa during the 2070s compared to the modern climate state (Gbode et al., 2021). The increase of ASM rainfall can be attributed to factors such as enhanced moisture convergence at low levels (e.g., D'Agostino et al., 2019, 2020; Kitoh et al., 2013; Lee & Wang, 2014) and a greater interhemispheric thermal contrast (e.g., Jones et al., 2013; Navarro et al., 2017). In contrast, some climate models project dryer futures in sub-regions of Africa, for example, the Atlantic coast (e.g., Biasutti, 2019; Delire et al., 2008; James et al., 2013) and in the Sahel region (e.g., Biasutti & Giannini, 2006), and some models show no obvious changes in ASM rainfall (e.g., D'Agostino et al., 2019). Even among models that show a consensus on the global warming-induced signal, there are wide disparities in the magnitude of rainfall changes and in the spatial and seasonal patterns (Biasutti, 2013; Rowell et al., 2016). Furthermore, Biasutti (2013) points out that the direct effect of CO_2 is to enhance the monsoon precipitation, while warmer sea surface temperature (indirect effect of CO_2) contributes to a drying over the Sahel area.

Previous studies (e.g., Akinsanola & Zhou, 2019a; D'Agostino et al., 2019, 2020) have found that under modern climate conditions and future scenarios, the influence of rising CO_2 on monsoon precipitation exhibits a dual nature: On one hand, it increases the atmospheric water vapor content, facilitating a greater moisture supply for precipitation formation, generally known as the "thermodynamic effect." On the other hand, it also weakens the intensity of monsoon circulation, hence contributing to a reduction in monsoon rainfall (commonly referred to as the "dynamic effect"). In the context of future global warming scenarios, the projected change in monsoon precipitation is attributed to the combined impacts of both thermodynamic and dynamic factors.

Past research on the effects of CO_2 has primarily based on simulations for modern climate states and future scenarios. A question is whether such influence of CO_2 is applicable to other climate states that differ significantly from the present. In a more recent model study based on AWIESM, Shi et al. (2023) have shown that increased greenhouse gas concentrations lead to a dryness in northern Africa as well as other Northern Hemisphere monsoon regions under the Last Glacial Maximum climate condition. However, using the same model, an increase in northern Africa precipitation is simulated in the future scenario compared to the historical period (Semmler et al., 2020). This indicates a climate-dependency of global warming on ASM rainfall. To gain insight into this subject, here we examine the influence of increasing CO_2 levels on African monsoon precipitation under various climate states. This is achieved through a series of sensitivity simulations, covering three warm interglacial periods and two cold glacial periods. Details on the model employed in the present study, as well as our experimental design, are given in Section 2. In Section 3, we illustrate our simulated results. Finally, we discuss and conclude in Section 4.

2. Methods

The model used in this study, AWIESM2, is a state-of-the-art Earth system model developed at the Alfred Wegener Institute (AWI) (Sidorenko et al., 2019). It consists of an atmospheric component, ECHAM6 (Stevens et al., 2013), which includes a land-surface component JSBACH representing dynamic vegetation with two types of bare surface and multiple plant functional types (Brovkin et al., 2009; C. Reick et al., 2013; C. H. Reick et al., 2021), as well as an ice-ocean model FESOM2 employing a multi-resolution dynamical core based on finite volume formulation (Danilov et al., 2017). The atmosphere grid applied in the present study is T63L47, which has a global mean spatial resolution of 1.875° with 47 vertical levels. A spatially variable resolution is used for the ice-ocean component (Figure S1 in Supporting Information S1), from about 100 km in the open ocean to 25 km over polar areas and 35 km for the equatorial belt and along coastlines. Vertically, there are 46 uneven layers in the ocean. We perform five equilibrium simulations using AWIESM2, including three interglacial periods (pre-industrial (PI), mid-Holocene (MH), and last interglacial (LIG)) and two glacial periods (Last Glacial Maximum (LGM) and Marine Isotope Stage 3 (MIS3)). Each simulation is followed by a $2 \times CO_2$ experiment (labeled as PI_CO_2, MH_CO_2, LIG_CO_2, LGM_CO_2, and $MIS3\_CO_2$). For further details on experimental design, please refer to the Supporting Information S1 (Text S1). Moreover, to examine the mechanisms driving changes in ASM precipitation, a moisture budget analysis is conducted, which has been employed extensively in a number of previous studies (e.g., Akinsanola & Zhou, 2019a; D'Agostino et al., 2019, 2020; Peng & Zhou, 2017; Trenberth & Guillemot, 1995). This approach is detailed in Text S2 in Supporting Information S1.

3. Result

3.1. Different Background Climates

Prior to examining the response of ASM to increased CO_2 levels, it is important to look at the contrasting features of the simulated June-July-August-September (JJAS) background climates across the five selected time periods. Following Shi, Werner, Krug, et al. (2022), we adjust the calendar for each experiment so that it matches the seasonal insolation cycle. The modeled global surface air temperature (GMT) during JJAS is 15.5°C, 15.6°C and 16.9°C for PI, MH and LIG, respectively, while a relatively lower JJAS-mean GMT is simulated for LGM (11.1°C) and MIS3 (13.0°C). The spatial anomalies in surface air temperatures during JJAS with respect to PI, as shown in Figure S2 in Supporting Information S1, indicate a prevailing warming for MH and LIG. This warming tendency is particularly prominent in the Northern Hemisphere. Conversely, the two glacial time periods exhibit a general cooling pattern. The most noticeable cooling in the LGM and MIS3 occurs in the Northern Hemisphere land-ice area due to the high albedo and elevation of the ice sheets, and also happens in the subpolar Southern Ocean where sea ice presents (Figure S3 in Supporting Information S1).

The simulated PI precipitation, shown in Figure S4 in Supporting Information S1, exhibits reasonable agreement with observational data (Adler et al., 2018), although local wet biases are observed during both boreal summer and winter at the respective location of the Intertropical Convergence Zone (ITCZ). Such biases are common and are also present in other models (Gent et al., 2011; Lin, 2007; Sidorenko et al., 2015). Changes in annual mean precipitation between our paleo and PI simulations are shown in Figure S5 in Supporting Information S1. There is increased rainfall over the ASM region during the MH and LIG, with the increase being more pronounced in the LIG than in the MH (Figures S5a and S5b in Supporting Information S1). Additionally, wetter conditions are observed in other Northern Hemisphere monsoon regions, such as North America and South Asia, associated with a northward displacement of the ITCZ. In general, our results align well with proxy-based precipitation records compiled by Bartlein et al. (2011) and Scussolini et al. (2019), although the model tends to slightly underestimate the wetting at certain sites in northern Africa and Eurasia. We also assess the model's performance in representing precipitation changes between LGM and PI using pollen records (Bartlein et al., 2011). Overall, both the model and the proxies agree on the pronounced dryness over most Northern Hemisphere continents (Figure S5c in Supporting Information S1). Our results on precipitation changes between MH, LIG, LGM, and PI are generally consistent with other PMIP4 models (Brierley et al., 2020; B. L. Otto-Bliesner et al., 2021; Kageyama et al., 2021). For MIS3, to the best of our knowledge, no comprehensive compilation of precipitation reconstructions is available. However, some individual site-based studies suggest wetter conditions in northern Africa during MIS3 compared to PI (Kuechler et al., 2013), which is in agreement with our model results (Figure S5d in Supporting Information S1).

For more detailed information on the simulated glacial/interglacial climate and its comparison with proxy records, please refer to Shi, Werner, Wang, et al. (2022) and Shi et al. (2023).

3.2. Responses of Africa Summer Monsoon Rainfall to Doubling CO_2

Rising CO_2 levels causes a consistent increase in GMT during JJAS across the 5 selected time periods, albeit with varying degrees of magnitude. In the context of interglacial conditions, doubling CO_2 leads to a rise in JJAS-mean GMT by around 2.1–2.3°C. This temperature difference is slightly greater for the 2 specific glacial periods under consideration, ranging around 2.4–2.5°C. Moreover, we detect more pronounced surface warming over colder surfaces (Figure S6 in Supporting Information S1), for example, the areas of ice sheets and marginal sea ice. In LGM_CO2 and MIS3_CO2, one intriguing feature is the warming over Southern Ocean south of 60°S where sea ice exists. This leads to a reduction in meridional thermal gradient in LGM_CO2 and MIS3_CO2. CO_2 increase also affects Arctic temperatures: all sensitivity experiments exhibit a polar amplification signature. This feature is particularly pronounced in LGM_CO2.

The responses of JJAS-mean Africa rainfall to CO_2 increase are illustrated in Figure 1. It is evident that for the three interglacial time periods, northern Africa experiences a more humid climate condition with higher CO_2 levels, though with varying magnitudes and spatial patterns. The western coastal subregion in PI_CO_2 and MH_CO_2 experiences the most pronounced increase in rainfall (Figures 1a and 1b), particularly over the Guinean area. An exception is the western Sahel where a slight dryness is obtained. In LIG_CO_2, precipitation increases substantially over the central-eastern Sahel and Sahara regions (Figure 1c), while decreases in an area close to the

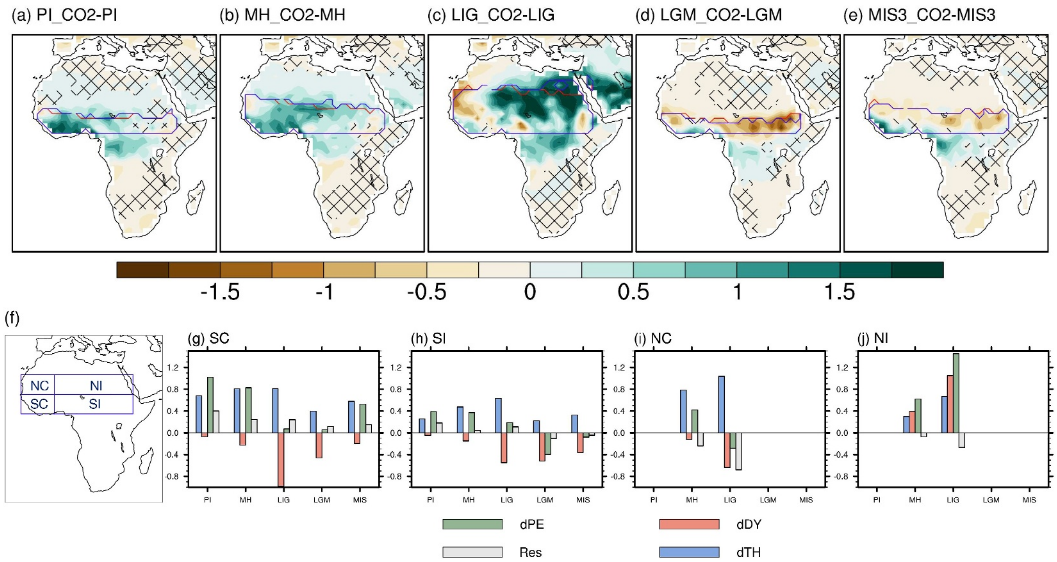

Figure 1. (a–e) Precipitation anomalies (mm/day) over Africa during JJAS for (a) PI_CO_2 minus PI, (b) MH_CO_2 minus MH, (c) LIG_CO_2 minus LIG, (d) LGM_CO_2 minus LGM, and (e) MIS3_CO_2 minus MIS3. Non-slashed areas indicate significant changes at 95% confidence level based on Student's *t* test. Areas within red (blue) lines represent ASM domains for reference (doubling CO_2) simulations. The ASM domain is defined as area with JJAS-minus-DJFM precipitation exceeding 2 mm/day, following D'Agostino et al. (2019). Boxes in (f) represent sub-regions of northern Africa. (g–j) Regionally averaged net precipitation (dPE) changes (mm/day), and changes in thermodynamic (dTH) and dynamic (dDY) components of the moisture budget, as well as its residual (Res) for (g) southern coastal region, (h) southern inland region, (i) northern coastal region, and (j) northern inland region. Note that only grid boxes within the ASM domain are considered, and values are only calculated if there are more than 20 grid boxed available.

North Atlantic coastline. In contrast, glacial simulations show a southward shift of the ITCZ and a general dryness in northern Africa due to increased CO_2, predominantly concentrated in the south of the Sahel region (Figures 1d and 1e).

3.3. Moisture Budget Decomposition

We also observe a spatial heterogeneity in the precipitation response to a doubling of CO_2 within the monsoon domain. In PI_CO_2 and MH_CO_2, the changes in precipitation appear to be more pronounced in the western region. In LIG_CO_2, contrast anomalies can be found between western coastal and interior regions, and changes in the subtropical zone are more prominent than those in the tropical areas. Moreover, despite a general tendency toward aridity, the western coastal region experiences a notable increase in precipitation in MIS3_CO_2 relative to MIS3.

Similar to Monerie et al. (2020), we divide the ASM area into 4 sub-regions (SC: southern coastal; NC: northern coastal; SI: southern inland; NI: northern inland, as seen in Figure 1f). To quantitatively understand the contrasting responses of ASM precipitation to the increase in CO_2 levels under interglacial and glacial boundary conditions and its spatial heterogeneity, we perform a moisture budget analysis (described in the Supporting Information S1). For each selected sub-region, the specific contribution of each component is calculated by averaging its values within the ASM domain in the corresponding sub-region. Here the ASM domain is defined as the area where the precipitation anomaly between JJAS and DJFM exceeds 2 mm/day (D'Agostino et al., 2019).

For all of the 4 sub-regions, the results indicate a positive impact on net precipitation resulting from the thermodynamic component (dTH, represented by the blue bars) in all experiments with rising CO_2 (Figures 1g–1j), attributed to an enrichment in atmospheric moisture content (Figures 2k–2o). Note that for the NC and NI regions, no data is provided for experiments PI, LGM, and MIS3, as the monsoon domains in these simulations are restricted to within 15°N. In the SC area, as shown in Figure 1g, while a negative impact from the dynamic term (dDY, depicted in red) is obtained for PI, MH and MIS, it is minor compared to the thermodynamic effect. Consequently, the wetter condition observed in SC in these simulations (referred to as dPE and depicted in green)

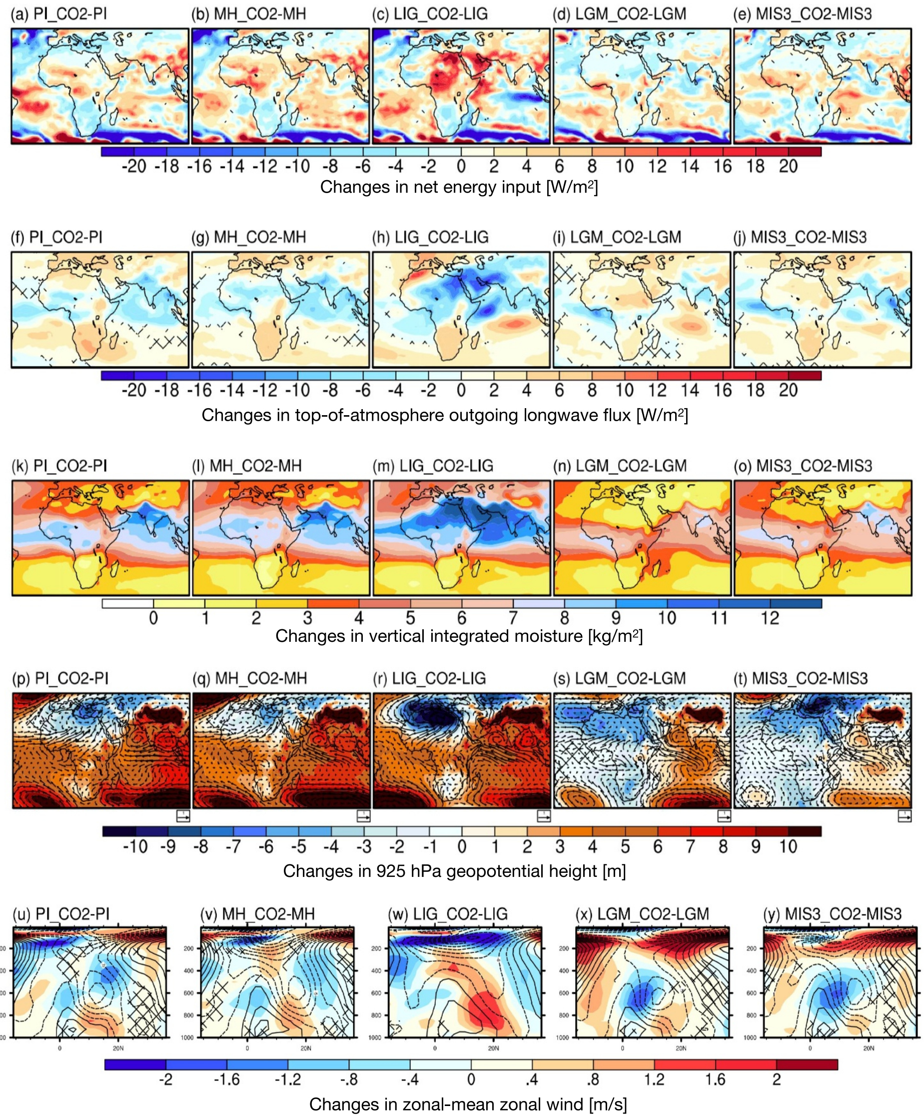

Figure 2. Anomalies in (a–e) JJAS net energy input (f–j) top-of-atmosphere outgoing longwave (W/m^2), (k–o) vertical integrated moisture (km/m^2), (p–t) 925 hPa geopotential height (m), and (u–y) zonal winds at all levels averaged over Africa, for (a, f, k, p, u) PI_CO_2 minus PI, (b, g, l, q, v) MH_CO_2 minus MH, (c, h, m, r, w) LIG_CO_2 minus LIG, (d, i, n, s, x) LGM_CO_2 minus LGM, and (e, j, o, t, y) MIS3_CO_2 minus MIS3. Non-slashed areas indicate significant changes at 95% confidence level based on Student's *t* test. Vectors in (p–t) represent 925 hPa winds anomalies (m/s). Contours in (u–y) are for Africa zonal winds at all levels in reference simulations.

is attributed to the dTH factor. During LIG and LGM, the thermodynamic and dynamic components in the SC region exhibit opposite effects of similar magnitude. Moreover, we observe a positive contribution from the transient eddies, represented by the residual term (Res). As a result, the slight increase in precipitation can be attributed to the combined effects of the thermodynamic (dTH) and the residual term (Res). This is also the case for LIG_CO_2 in the SI region (Figure 1h). In the SI zone (Figure 1h), all simulations with rising CO_2 again yield a negative contribution from the dynamic components. Nonetheless, the changes in net precipitation under glacial and interglacial conditions are contrary: in LGM_CO_2 and MIS3_CO_2, substantial negative contribution exerted by dDY overpowers the positive contribution stemming from dTH and therefore dominates a reduction in net precipitation. Whereas in interglacial climates except the LIG_CO_2, the dynamic term plays a minor role, and the positive dTH factor leads to a more humid condition. This is similarly applicable to MH in the NC region (Figure 1i). In LIG_CO_2, thermodynamic and dynamic factors mutually reinforce each other in the NI area

(Figure 1j), resulting in a great wettening tendency. Conversely, the NC area in LIG_CO_2 experiences a reduction in monsoon rainfall compared to LIG, most attributed to the dynamic and residual components. This highlights prominent influences from the atmospheric mean flow and transient eddies. The spatial pattern (Figure S7 in Supporting Information S1) demonstrates a dipole change in the dynamic component for the Last interglacial, which generally exerts a negative (positive) influence on net precipitation across tropical (northern) Africa, implying a northward shift of the atmospheric mean flow.

Given above, the striking contrast in the ASM rainfall response to rising CO_2 during glacial and interglacial periods is intricately connected to the dynamic component. While the dynamic component predominantly influences the anomalous moisture budget in most African monsoon regions in glacial experiments (particularly the SI region), it bears lesser significance in interglacial simulations. Therefore, examining the dDY term is key to understanding the contrast responses of ASM rainfall under global warming.

3.4. Mechanisms of the dDY

Since the dDY term is associated with changes in tropical circulation, in the following analysis, we focus on two important relevant factors: the tropical overturning (i.e., the ascending branch of the Southern Hemisphere Hadley cell) and the African easterly jet (AEJ). Both are key processes affecting the ASM dynamics.

3.4.1. Tropical Overturning

It is widely acknowledged that the tropical atmospheric mass flux experiences a decline in strength as a result of rising temperatures, typically coinciding with a reduction in the intensity of the ascending branch of the Hadley circulation (D'Agostino et al., 2017; Lionello et al., 2024). The weakening of the tropical overturning can be attributed to certain complementary thermodynamic constraints. One such constraint is the faster increase in tropical dry static stability compared to subtropical radiative cooling (Knutson & Manabe, 1996), another is the slower increase of the global hydrological cycle compared to lower tropospheric water vapor (Held & Soden, 2006). The modeled reduction in tropical overturning in most of our experiments with rising CO_2 aligns well with previous findings (Figure S8 in Supporting Information S1). One exception is the LIG_CO2 experiment which presents the opposite (Figure S8c in Supporting Information S1). We also observe that the tropical ascent in the LGM_CO_2 and MIS3_CO_2 exhibits a more pronounced weakening compared to PI_CO_2 and MH_CO_2.

In order to understand the distinct tropical overturning responses associated with rising CO_2 levels in different climates, here we analyze changes in the net energy input (NEI) into the atmosphere (i.e., the difference in radiative fluxes between the top-of-atmosphere and the Earth's surface) (Figures 2a–2e). Evident from Figure 2c, compared to LIG, the NEI anomaly in LIG_CO_2 exhibits predominantly positive values across southern Eurasia and the majority of northern Africa, particularly in the central-eastern area (e.g., the NI and SI subregions). To compensate for these changes in NEI, more energy should be transported away through a strengthening of the atmospheric circulation in LIG_CO_2. Whereas for experiments PI_CO_2, MH_CO_2, LGM_CO_2 and MIS_CO_2, in the absence of such strong land-sea NEI contrast (Figures 2a and 2b), the increased static stability dominates a weakening in the tropical circulation. In a warming climate, static stability in the tropics increases as the strength of the hydrological cycle increases more slowly than does the moisture near the surface (Held & Soden, 2006). In the LGM_CO_2 experiments, the increase in NEI is even more pronounced in the tropical oceans compared to continents, as LGM_CO_2 exhibits a decrease in NEI over northern Africa and a simultaneous increase in NEI over the adjacent oceans to the south.

Another factor affecting the tropical circulation is the change in interhemispheric contrast in NEI. Such a change necessitates anomalous meridional energy transport to restore energy balance. During summer, most of this transport is facilitated by monsoonal circulations (D'Agostino et al., 2019; Heaviside & Czaja, 2013; Walker, 2017). As a result, this would lead to a shift of the monsoonal circulation's ascending branches and precipitation maxima toward the hemisphere with higher NEI, along with a potential strengthening of the circulation (Bischoff et al., 2017; D'Agostino et al., 2017; T. Schneider et al., 2014). Here we calculate for each experiment the interhemispheric contrast in NEI in the tropics, defined as the NEI difference between 0 and 30°N and 0–30°S. Only LIG_CO_2 shows an enhanced interhemispheric NEI contrast compared to its reference climate, with an anomaly of 1.1 W/m^2, while other experiments configured with rising CO_2 show a negative change

(−0.18 W/m^2 for PI_CO_2-PI; −0.67 W/m^2 for MH_CO_2-MH; −1.29 W/m^2 for LGM_CO_2-LGM; and −0.39 W/m^2 for MIS_CO_2-MIS).

To gain an understanding of why the continental NEI and interhemispheric NEI contrast specifically increases only in the LIG_CO_2 experiment, we conduct further analysis for the individual component contributing to the NEI. This involves examining the top-of-atmosphere radiative fluxes and the radiative and turbulent fluxes at the surface. Our analysis revealed that an important factor responsible for the NEI changes in LIG_CO_2 is a decrease in outgoing longwave flux at the top of the atmosphere, specifically observed over northern Africa (mostly in the NI and SI subregions) and southern Eurasia (Figure 2h). This reduction in longwave flux can be attributed to an increase in water vapor in the atmosphere column (Figure 2m), which absorbs more longwave flux. Then another question arises: why is there such a pronounced increase in the water vapor exclusively in the LIG_CO_2 experiment? Due to orbital configuration, the Northern Hemisphere summer insolation in LIG is much stronger compared to other reference experiments (PI, MH, LGM, and MIS3), facilitating a deeper monsoon system (see contours in Figures 2u–2y, the top of the monsoon layer is where the zonal wind component equals zero, going from westerly downward to easterly upward) and a stronger Saharan Heat Low (SHL) (a large-scale area of low pressure, high temperatures, and dry air over northern Africa, Figure S9 in Supporting Information S1). The rise of CO_2 levels further increases the monsoon depth in LIG_CO_2 (shadings in Figure 2w). Additionally, it promotes a pronounced anomalous low pressure system north of 25°N (i.e., an enhanced SHL) and westerlies along its southern flank (Figure 2r). This impact is relatively minor in other sensitivity experiments (Figures 2p, 2q, 2s, and 2t). Therefore, the increased intensity and expanded vertical range of the westerly winds in LIG_CO_2 facilitate a more efficient transportation of moisture from the Atlantic Ocean to Africa.

Though a doubling of CO_2 introduces a global warming in our sensitivity simulations at similar degrees (2.1–2.5°C), the increase in atmospheric moisture is significantly smaller in LGM_CO_2 and MIS_CO_2 compared to the interglacial experiments (Figures 2k–2o), which provides a constraint on the thermodynamic influence of CO_2. This is principally attributable to the non-linear correlation between temperature and moisture content. Specifically, as temperature rises, so does saturation vapor pressure of water vapor. Therefore, humidity rises less in colder climates for the same temperature increase compared to warmer climates.

A reduced temperature gradient between the tropics and the extratropics has a weakening effect on the strength of the Hadley cell (D'Agostino et al., 2017), and the African summer monsoon is closely linked to the ascending branch of the Hadley cell. Such a decrease in tropic-extratropic temperature gradient is seen in the Northern Hemisphere in all experiments, as the continents and ice sheets experience more warming than the tropical areas (Figure S6 in Supporting Information S1). For the Southern Hemisphere, however, the most pronounced warming happens over sea ice-covered regions (Figures S6d and S6e in Supporting Information S1). Notably, only the glacial experiments show an extensive sea ice extent that reaches the extratropics, as far north as 50°S in the Atlantic sector (Figure S3 in Supporting Information S1). The enhanced warming of the extratropical sea ice areas in the glacial simulations results in a reduction of the tropic-extratropic temperature gradient, which in turn weakens the Hadley circulation.

3.4.2. African Easterly Jet (AEJ)

Over northern Africa, the SHL fosters a high-pressure system above (i.e., the Saharan high), with its core typically located at around 600 hPa. Along the southern edge of the Saharan High, strong easterly winds, known as the African Easterly Jet (AEJ), emerge as a result of Coriolis accelerations acting on the northerly outflow from the Saharan High system. Previous studies have indicated that the AEJ plays a crucial role in regulating northern Africa precipitation by carrying moisture away from the continent below the condensation level, thus reducing moisture supply over northern Africa (e.g., Cook, 1999; Rachmayani et al., 2015; Rowell, 2003). The Saharan High weakens in LIG_CO_2 (Figure 3c). Meanwhile, the 600 hPa geopotential height increases over tropical Africa. This dipole pattern implies a decline in the north-south pressure gradient, leading to a weakened AEJ (Figure 3h). As a consequence, positive anomalous inland moisture transport presents over northern Africa in LIG_CO_2 (Figure 3m). The weakened Saharan High and AEJ are also associated with a vertical expansion of the monsoon system. During the LIG, the ASM is both stronger and deeper (Figure 2w) compared to other reference experiments. The increase in CO_2 further amplifies the monsoon system, with this effect being more pronounced in LIG_CO_2 than in the other simulations. In LIG_CO_2, the AMS not only expands northward but also extends

10.1029/2024GL112717

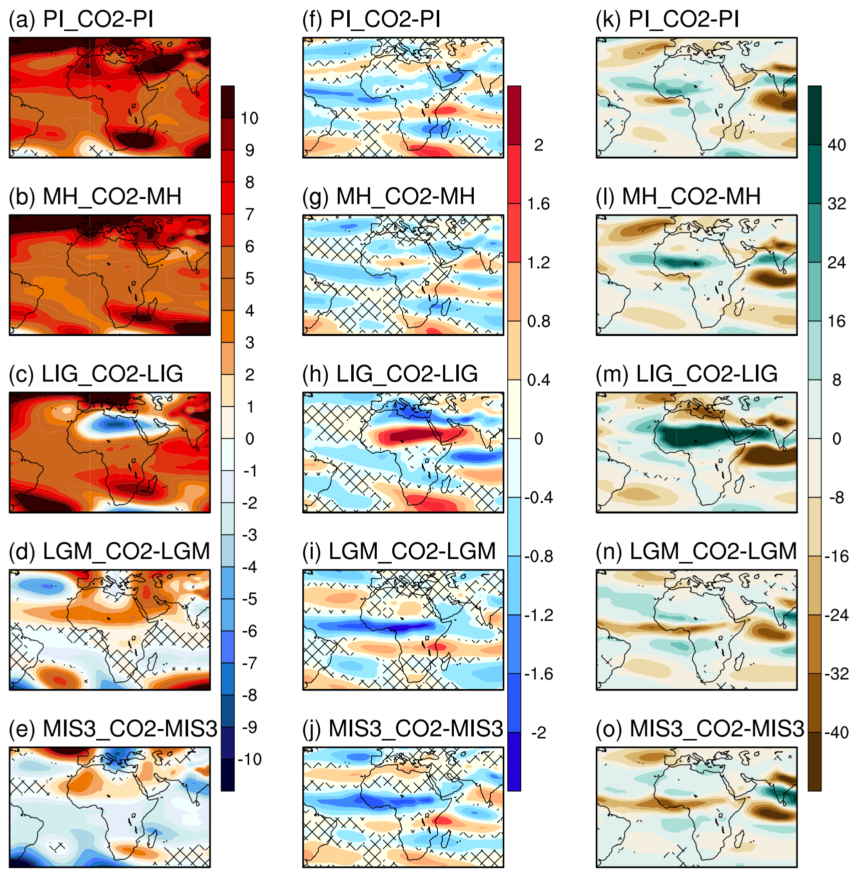

Figure 3. Anomalies in (a–e) 600 hPa geopotential height, (f–j) 600 hPa zonal wind (westerlies positive), and (k–o) vertical integrated zonal moisture flux, for (a, f, k) PI_CO_2 minus PI, (b, g, l) MH_CO_2 minus MH, (c, h, m) LIG_CO_2 minus LIG, (d, i, n) LGM_CO_2 minus LGM, and (e, j, o) MIS3_CO_2 minus MIS3. Units: m, m/s, and kg/(ms).

vertically, introducing anomalous negative pressure and westerly winds at the 600 hPa level. Conversely, for the glacial experiments with rising CO_2 (i.e., LGM_CO_2 and MIS3_CO_2), the Saharan high, meridional pressure gradient, and AEJ are all enhanced (Figures 3d, 3e, 3i, and 3j). This results in more moisture being exported from inland toward the west coast (Figures 3n and 3o). In PI_CO_2 and MH_CO_2, the changes in AEJ are relatively minor (Figures 3f and 3g) due to small changes in meridional contrast in geopotential heights (Figures 3a and 3b). Thus, the enhanced ocean-to-land moisture transport in PI_CO_2 and MH_CO_2 as seen in Figures 3k and 3l is mainly a result of increased water vapor in the atmosphere rather than atmospheric circulation changes.

3.5. Role of the Atlantic Meridional Overturning Circulation (AMOC)

The Atlantic Meridional Overturning Circulation (AMOC) plays a crucial role in modulating precipitation patterns over northern Africa, with its influence on regional climate variability on millennial timescales being potentially comparable to that of changes in insolation (Menviel et al., 2021). Our results reveal a significant weakening of the AMOC in the PI_CO_2, MH_CO_2, and LIG_CO_2 simulations, with a reduction of 5.1 Sv, 3.7 Sv, and 3.86 Sv, respectively (Figure S10 in Supporting Information S1). The weakening of AMOC is a well-documented response to global warming and is consistently reproduced in most climate model projections (Bellomo et al., 2021; Cheng et al., 2013). It is associated with reduced meridional oceanic heat transport to the North Atlantic, which leads to a cooling of the North Atlantic and a warming of the South Atlantic. This interhemispheric energy asymmetry, superimposed on the broader CO_2-induced global warming (Figure S6 in Supporting Information S1), results in less evaporation from the North Atlantic, reduced ocean-to-land moisture transport, and a southward displacement of the ITCZ (Ben-Yami et al., 2024; Kageyama et al., 2013; Lionello et al., 2024; Stouffer et al., 2006) due to atmospheric cross-equatorial energy regulation accomplished by Hadley circulation (Nicknish et al., 2023). These changes contribute to drier conditions in northern Africa.

Our model results further support the positive correlation between the AMOC strength and precipitation in the African monsoon system (Figure S11 in Supporting Information S1). However, in glacial simulations with rising CO_2, while the AMOC becomes shallower, there is no substantial change in its overall strength, suggesting that the AMOC's response to CO_2 is climate-dependent. Given above, during interglacial periods, the weakened AMOC appears to limit the moisture availability for the ASM, thereby dampening the response of precipitation to rising CO_2. In contrast, under glacial conditions, where no significant AMOC weakening occurs in response to CO_2, the ASM precipitation response is primarily governed by atmospheric processes rather than oceanic feedbacks.

4. Discussion and Conclusions

Previous studies have shown that, the increase in carbon dioxide (CO_2) levels leads to more precipitation in the monsoon regions, as a result of increased amount of atmospheric water vapor (e.g., Akinsanola & Zhou, 2019a; D'Agostino et al., 2019, 2020). This is typically known as the "thermodynamic effect." However, in a warmer climate, static stability in the tropics increases, favoring a weakening in tropical circulation (Knutson & Manabe, 1996; Held & Soden, 2006; D'Agostino et al., 2017) and a decrease in monsoon strength (the "dynamic effect"). Hence, the ultimate change of monsoon rainfall results from a balance between the thermodynamic and dynamic effects. However, there remains a lack of knowledge due to the linear combination of CO_2 increase with other boundary conditions on the relative importance of thermodynamic and dynamic effects. In this respect, the question is arguing because the climate mean state can influence the atmospheric response in a surprising way. In the present study, we perform double-CO_2 experiments under various climate conditions, encompassing three interglacial (PI, MH, and LIG), and 2 glacial periods (LGM and MIS3). Through these experiments, we reveal that the African monsoon response to global warming depends on the background climate state. Our model results suggest that under warm interglacial climate states, northern Africa experiences increased precipitation as a result of rising CO_2, whereas the opposite case is found for the cold glacial states. In our interglacial experiments, it is observed that an increase in atmospheric moisture is the main contributor to the wetter conditions in the ASM area. Whereas, our glacial experiments reveal that the overwhelming factor impacting ASM precipitation is the "dynamic effect" associated with rising CO_2 levels. This dynamic effect leads to a slowdown in tropical circulation, ultimately resulting in reduced precipitation in the ASM region. Moreover, a spatial heterogeneity in the precipitation responses to increased CO_2 is observed. Under glacial climates, the reduced rainfall in the ASM domain due to increased CO_2 is mostly restricted to the interior continent, influenced by a negative contribution from the "dynamic effect." Conversely, the western coastal region experiences a generally wetter condition due to the "thermodynamic effect." Under PI and MH climates, an increase in CO_2 leads to enhanced precipitation across the majority of the ASM region, primarily attributed to the "thermodynamic effect"; however, this response is markedly more pronounced in the western coastal area compared to the central and eastern regions. Under last interglacial state, the ASM domain is dominated by an enhancement in monsoon precipitation, this stems from a mutual reinforcement of both dynamic and thermodynamic factors. However, a specific region in western coastal Africa that exhibits a clear drying tendency, resulted from changes in atmospheric circulation and transient eddies.

The observed decline in the tropical circulation as simulated in most of our experiments with rising CO_2 coincides with an expansion and weakening of the atmospheric circulation under global warming suggested by previous studies suggesting (D'Agostino et al., 2017; Gastineau et al., 2008; Hu et al., 2018; Lionello et al., 2024; Lu et al., 2007; Yang et al., 2020, 2023). The degree of this weakening is relatively greater in our glacial simulations than that in the interglacial experiments. The negative contribution from the dynamic term in the glacial simulations dominates over the increase in specific humidity (i.e., the thermodynamic term) on the rainfall changes. Another intriguing feature in our model study is the strengthening in the ascending branch of the Hadley circulation caused by rising levels of CO_2 under warm LIG climate condition. This strengthening is caused by an increase in Net Energy Input (NEI) over Northern Hemisphere subtropical continents, especially northern Africa, Saudi Arabia, Indian and South China, as well as an enhanced interhemisphere NEI contrast. The spatial pattern of dDY component for LIG_CO2 exhibits a drying tendency in the Sahel region (Figure S7 in Supporting Information S1), implying a decrease in moisture convergence related to a weakened atmospheric mean flow. However, compared to the other experiments, the northern border of ASM domain in LIG expands significantly to approximately 20°N, and monsoon areas outside the Sahel region are dominated by positive dDY values. The dipole pattern of dDY is associated with a northward shift of the tropical circulation. In our glacial simulations with rising CO_2 levels, no pronounced contrast is found for NEI changes over tropical oceans and northern Africa. This fact, together with a strong warming over regions south of 60°S that largely diminishes the meridional temperature gradient, as well as a decreased interhemisphere NEI contrast, are responsible for the substantial weakening in tropical overturning.

The results in the present study are based on idealized model simulations that solely focus on changes in CO_2 concentration. However, in reality, CO_2 cannot be the exclusive variable boundary condition. At a glacial-interglacial time scale, especially, alterations in greenhouse gases are often accompanied by concurrent changes in sea level and ice sheets, which can also exert a significant influence on ASM precipitation. For example, the presence of the Laurentide and Scandinavian ice sheets is an important factor in forming a dry climate during the LGM (Cao et al., 2019; Shi et al., 2023). Additionally, sea level rise and subsequent reduction in continental area have been simulated to induce drying in the ASM region (refer to Figure 7f in Cao et al., 2019). It is therefore anticipated that during deglaciation periods, changes in ASM precipitation are regulated by the combined effects from increased CO_2 concentration, rising sea levels, and reduced ice sheet elevation.

In addition to atmospheric factors, the oceanic processes can also have an important influence on the African precipitation. Using an intermediate climate model, an "upped-ante mechanism" was identified: when greenhouse gases increase, a warmer troposphere raises the threshold of surface boundary layer moisture necessary for convection to occur (Neelin et al., 2003). This threshold can be achieved with adequate moisture supply, with one important moisture source region being the subtropical North Atlantic. A North Atlantic Relative Index (NARI) has been introduced (Giannini et al., 2013), defined as the difference between SST averaged across the subtropical North Atlantic (10°N–40°N, 75°W–15°W) and the global tropical oceans (20°S–20°N). Model projections indicated a robust correlation between the NARI and variability in Sahel rainfall (Giannini et al., 2013; Giannini & Kaplan, 2019). Similarly, our simulations suggest a general linear relationship between ASM precipitation and NARI (Figure S12 in Supporting Information S1). Moreover, the AMOC shows varying responses across different experiments: weakened AMOC is obtained in the three interglacial simulations (PI_CO_2, MH_CO_2, and LIG_CO_2), favoring less ASM precipitation and therefore dampening the effect of rising CO_2. In contrast, under glacial boundary conditions, the ASM precipitation response to CO_2 is driven mainly by atmospheric processes due to the rather small change in the strength of AMOC.

To conclude, our model results agree with previous studies on the fact that the response of the African summer monsoon precipitation to increasing CO_2 concentration is contingent upon a compensation between the thermodynamic and dynamic effects. We further find that the degree of such compensation depends significantly on the background climate configurations (e.g., orbital parameters, ice sheets, sea ice, etc). This study enhances our comprehension of the intricate relationship between global warming, thermodynamic processes, and dynamic processes in influencing rainfall patterns during the African summer monsoon phase. It also emphasizes the significance of taking into account specific climatic periods and evaluating the varying impacts of different mechanisms when analyzing the effects of CO_2 on monsoon systems.

Data Availability Statement

The model outputs related to the present study are available on Zenodo repository (Shi, 2024).

Acknowledgments

This study is supported by the Southern Marine Science and Engineering Guangdong Laboratory (Zhuhai) (Grant SML2023SP204), the Ocean Negative Carbon Emissions (ONCE) Program, and the National Natural Science Foundation of China (NSFC) (Grants 42206256; 42488201). The simulations were conducted on Deutsche Klimarechenzentrum (DKRZ). Open Access funding enabled and organized by Projekt DEAL.

References

Adler, R. F., Sapiano, M. R., Huffman, G. J., Wang, J.-J., Gu, G., Bolvin, D., et al. (2018). The global precipitation climatology project (GPCP) monthly analysis (new version 2.3) and a review of 2017 global precipitation. *Atmosphere*, *9*(4), 138. https://doi.org/10.3390/atmos9040138

Akinsanola, A., & Zhou, W. (2019a). Ensemble-based CMIP5 simulations of West African summer monsoon rainfall: Current climate and future changes. *Theoretical and Applied Climatology*, *136*(3–4), 1021–1031. https://doi.org/10.1007/s00704-018-2516-3

Akinsanola, A., & Zhou, W. (2019b). Projection of West African summer monsoon rainfall in dynamically downscaled CMIP5 models. *Climate Dynamics*, *53*(1–2), 81–95. https://doi.org/10.1007/s00382-018-4568-6

Akinsanola, A., Zhou, W., Zhou, T., & Keenlyside, N. (2020). Amplification of synoptic to annual variability of West African summer monsoon rainfall under global warming. *Npj Climate and Atmospheric Science*, *3*(1), 21. https://doi.org/10.1038/s41612-020-0125-1

Bartlein, P. J., Harrison, S., Brewer, S., Connor, S., Davis, B., Gajewski, K., et al. (2011). Pollen-based continental climate reconstructions at 6 and 21 ka: A global synthesis. *Climate Dynamics*, *37*(3), 775–802. https://doi.org/10.1007/s00382-010-0904-1

Bellomo, K., Angeloni, M., Corti, S., & von Hardenberg, J. (2021). Future climate change shaped by inter-model differences in Atlantic meridional overturning circulation response. *Nature Communications*, *12*(1), 1–10. https://doi.org/10.1038/s41467-021-24015-w

Ben-Yami, M., Good, P., Jackson, L., Crucifix, M., Hu, A., Saenko, O., et al. (2024). Impacts of AMOC collapse on monsoon rainfall: A multi-model comparison. *Earth's Future*, *12*(9), e2023EF003959. https://doi.org/10.1029/2023ef003959

Biasutti, M. (2013). Forced Sahel rainfall trends in the CMIP5 archive. *Journal of Geophysical Research: Atmospheres*, *118*(4), 1613–1623. https://doi.org/10.1002/jgrd.50206

Biasutti, M. (2019). Rainfall trends in the African Sahel: Characteristics, processes, and causes. *Wiley Interdisciplinary Reviews: Climate Change*, *10*(4), e591. https://doi.org/10.1002/wcc.591

Biasutti, M., & Giannini, A. (2006). Robust Sahel drying in response to late 20th century forcings. *Geophysical Research Letters*, *33*(11). https://doi.org/10.1029/2006gl026067

Bischoff, T., Schneider, T., & Meckler, A. N. (2017). A conceptual model for the response of tropical rainfall to orbital variations. *Journal of Climate*, *30*(20), 8375–8391. https://doi.org/10.1175/jcli-d-16-0691.1

Brierley, C., Zhao, A., Harrison, S. P. e. a., Braconnot, P., Williams, C. J. R., Thornalley, D. J. R., et al. (2020). Large-scale features and evaluation of the PMIP4-CMIP6 midHolocene simulations. *Climate of the Past*, *16*(5), 1847–1872. https://doi.org/10.5194/cp-16-1847-2020

Brovkin, V., Raddatz, T., Reick, C. H., Claussen, M., & Gayler, V. (2009). Global biogeophysical interactions between forest and climate. *Geophysical Research Letters*, *36*(7). https://doi.org/10.1029/2009gl037543

Cao, J., Wang, B., & Liu, J. (2019). Attribution of the last glacial maximum climate formation. *Climate Dynamics*, *53*(3), 1661–1679. https://doi.org/10.1007/s00382-019-04711-6

Cheng, W., Chiang, J. C., & Zhang, D. (2013). Atlantic meridional overturning circulation (AMOC) in cmip5 models: Rcp and historical simulations. *Journal of Climate*, *26*(18), 7187–7197. https://doi.org/10.1175/jcli-d-12-00496.1

Cook, K. H. (1999). Generation of the African easterly jet and its role in determining West African precipitation. *Journal of Climate*, *12*(5), 1165–1184. https://doi.org/10.1175/1520-0442(1999)012<1165:gotaej>2.0.co;2

D'Agostino, R., Bader, J., Bordoni, S., Ferreira, D., & Jungclaus, J. (2019). Northern hemisphere monsoon response to mid-Holocene orbital forcing and greenhouse gas-induced global warming. *Geophysical Research Letters*, *46*(3), 1591–1601. https://doi.org/10.1029/2018gl081589

D'Agostino, R., Brown, J. R., Moise, A., Nguyen, H., Silva Dias, P. L., & Jungclaus, J. (2020). Contrasting southern hemisphere monsoon response: MidHolocene orbital forcing versus future greenhouse gas–induced global warming. *Journal of Climate*, *33*(22), 9595–9613. https://doi.org/10.1175/jcli-d-19-0672.1

D'Agostino, R., Lionello, P., Adam, O., & Schneider, T. (2017). Factors controlling Hadley circulation changes from the last glacial maximum to the end of the 21st century. *Geophysical Research Letters*, *44*(16), 8585–8591. https://doi.org/10.1002/2017gl074533

Danilov, S., Sidorenko, D., Wang, Q., & Jung, T. (2017). The finite-volume sea ice–ocean model (FESOM2). *Geoscientific Model Development*, *10*(2), 765–789. https://doi.org/10.5194/gmd-10-765-2017

Delire, C., Ngomanda, A., & Jolly, D. (2008). Possible impacts of 21st century climate on vegetation in central and west africa. *Global and Planetary Change*, *64*(1–2), 3–15. https://doi.org/10.1016/j.gloplacha.2008.01.008

Dosio, A., Jury, M. W., Almazroui, M., Ashfaq, M., Diallo, I., Engelbrecht, F. A., et al. (2021). Projected future daily characteristics of African precipitation based on global (CMIP5, CMIP6) and regional (CORDEX, CORDEX-CORE) climate models. *Climate Dynamics*, *57*(11), 3135–3158. https://doi.org/10.1007/s00382-021-05859-w

Dosio, A., & Panitz, H.-J. (2016). Climate change projections for CORDEX-Africa with COSMO-CLM regional climate model and differences with the driving global climate models. *Climate Dynamics*, *46*(5–6), 1599–1625. https://doi.org/10.1007/s00382-015-2664-4

Gaetani, M., Flamant, C., Bastin, S., Janicot, S., Lavaysse, C., Hourdin, F., et al. (2017). West African monsoon dynamics and precipitation: The competition between global SST warming and CO_2 increase in CMIP5 idealized simulations. *Climate Dynamics*, *48*(3–4), 1353–1373. https://doi.org/10.1007/s00382-016-3146-z

Gastineau, G., Treut, H. L., & Li, L. (2008). Hadley circulation changes under global warming conditions indicated by coupled climate models. *Tellus A: Dynamic Meteorology and Oceanography*, *60*(5), 863–884. https://doi.org/10.1111/j.1600-0870.2008.00344.x

Gbode, I. E., Ogunjobi, K. O., Dudhia, J., Ajayi, V. O., & Liu, C. (2021). Impacts of global warming on West African monsoon rainfall: Downscaling by pseudo global warming method. *Atmospheric Research*, *249*, 105334. https://doi.org/10.1016/j.atmosres.2020.105334

Gent, P. R., Danabasoglu, G., Donner, L. J., Holland, M. M., Hunke, E. C., Jayne, S. R., et al. (2011). The Community Climate System Model version 4. *Journal of Climate*, *24*(19), 4973–4991. https://doi.org/10.1175/2011jcli4083.1

Giannini, A., & Kaplan, A. (2019). The role of aerosols and greenhouse gases in Sahel drought and recovery. *Climatic Change*, *152*(3), 449–466. https://doi.org/10.1007/s10584-018-2341-9

Giannini, A., Salack, S., Lodoun, T., Ali, A., Gaye, A., & Ndiaye, O. (2013). A unifying view of climate change in the Sahel linking intra-seasonal, interannual and longer time scales. *Environmental Research Letters*, *8*(2), 024010. https://doi.org/10.1088/1748-9326/8/2/024010

He, C., Li, T., & Zhou, W. (2020). Drier North American monsoon in contrast to Asian–African monsoon under global warming. *Journal of Climate*, *33*(22), 9801–9816. https://doi.org/10.1175/jcli-d-20-0189.1

Heaviside, C., & Czaja, A. (2013). Deconstructing the Hadley cell heat transport. *Quarterly Journal of the Royal Meteorological Society*, *139*(677), 2181–2189. https://doi.org/10.1002/qj.2085

Held, I. M., & Soden, B. J. (2006). Robust responses of the hydrological cycle to global warming. *Journal of Climate*, *19*(21), 5686–5699. https://doi.org/10.1175/jcli3990.1

Hu, Y., Huang, H., & Zhou, C. (2018). Widening and weakening of the Hadley circulation under global warming. *Science Bulletin*, *63*(10), 640–644. https://doi.org/10.1016/j.scib.2018.04.020

James, R., & Washington, R. (2013). Changes in African temperature and precipitation associated with degrees of global warming. *Climatic Change*, *117*(4), 859–872. https://doi.org/10.1007/s10584-012-0581-7

James, R., Washington, R., & Rowell, D. P. (2013). Implications of global warming for the climate of African rainforests. *Philosophical Transactions of the Royal Society B: Biological Sciences*, *368*(1625), 20120298. https://doi.org/10.1098/rstb.2012.0298

Jones, G. S., Stott, P. A., & Christidis, N. (2013). Attribution of observed historical near–surface temperature variations to anthropogenic and natural causes using CMIP5 simulations. *Journal of Geophysical Research: Atmospheres*, *118*(10), 4001–4024. https://doi.org/10.1002/jgrd.50239

Kageyama, M., Harrison, S. P., Kapsch, M.-L., Lofverstrom, M., Lora, J. M., Mikolajewicz, U., et al. (2021). The PMIP4 last glacial maximum experiments: Preliminary results and comparison with the PMIP3 simulations. *Climate of the Past*, *17*(3), 1065–1089. https://doi.org/10.5194/cp-17-1065-2021

Kageyama, M., Merkel, U., Otto-Bliesner, B., Prange, M., Abe-Ouchi, A., Lohmann, G., et al. (2013). Climatic impacts of fresh water hosing under last glacial maximum conditions: A multi-model study. *Climate of the Past*, *9*(2), 935–953. https://doi.org/10.5194/cp-9-935-2013

Kitoh, A., Endo, H., Krishna Kumar, K., Cavalcanti, I. F., Goswami, P., & Zhou, T. (2013). Monsoons in a changing world: A regional perspective in a global context. *Journal of Geophysical Research: Atmospheres*, *118*(8), 3053–3065. https://doi.org/10.1002/jgrd.50258

Knutson, T., & Manabe, S. (1996). Time-mean response over the tropical pacific to increased CO_2 in a coupled ocean-atmosphere model. *Oceanographic Literature Review*, *10*(43), 974.

Kuechler, R., Schefuß, E., Beckmann, B., Dupont, L., & Wefer, G. (2013). NW African hydrology and vegetation during the Last Glacial cycle reflected in plant-wax-specific hydrogen and carbon isotopes. *Quaternary Science Reviews*, *82*, 56–67. https://doi.org/10.1016/j.quascirev.2013.10.013

Laprise, R., Hernández-Díaz, L., Tete, K., Sushama, L., Šeparović, L., Martynov, A., et al. (2013). Climate projections over CORDEX Africa domain using the fifth-generation Canadian regional climate model (CRCM5). *Climate Dynamics*, *41*(11–12), 3219–3246. https://doi.org/10.1007/s00382-012-1651-2

Lee, J.-Y., & Wang, B. (2014). Future change of global monsoon in the CMIP5. *Climate Dynamics*, *42*(1–2), 101–119. https://doi.org/10.1007/s00382-012-1564-0

Lin, J.-L. (2007). The double-ITCZ problem in IPCC AR4 coupled GCMs: Ocean–atmosphere feedback analysis. *Journal of Climate*, *20*(18), 4497–4525. https://doi.org/10.1175/jcli4272.1

Lionello, P., D'Agostino, R., Ferreira, D., Nguyen, H., & Singh, M. S. (2024). The Hadley circulation in a changing climate. *Annals of the New York Academy of Sciences*, *1534*(1), 69–93. https://doi.org/10.1111/nyas.15114

Lu, J., Vecchi, G. A., & Reichler, T. (2007). Expansion of the Hadley cell under global warming. *Geophysical Research Letters*, *34*(6). https://doi.org/10.1029/2006gl028443

Maynard, K., Royer, J.-F., & Chauvin, F. (2002). Impact of greenhouse warming on the West African summer monsoon. *Climate Dynamics*, *19*(5–6), 499–514. https://doi.org/10.1007/s00382-002-0242-z

Menviel, L., Govin, A., Avenas, A., Meissner, K. J., Grant, K. M., & Tzedakis, P. C. (2021). Drivers of the evolution and amplitude of African humid periods. *Communications Earth & Environment*, *2*(1), 237. https://doi.org/10.1038/s43247-021-00309-1

Monerie, P.-A., Sanchez-Gomez, E., Gaetani, M., Mohino, E., & Dong, B. (2020). Future evolution of the Sahel precipitation zonal contrast in CESM1. *Climate Dynamics*, *55*(9), 2801–2821. https://doi.org/10.1007/s00382-020-05417-w

Navarro, J. C. A., Ekman, A. M., Pausata, F. S., Lewinschal, A., Varma, V., Seland, Ø., et al. (2017). Future response of temperature and precipitation to reduced aerosol emissions as compared with increased greenhouse gas concentrations. *Journal of Climate*, *30*(3), 939–954. https://doi.org/10.1175/jcli-d-16-0466.1

Neelin, J., Chou, C., & Su, H. (2003). Tropical drought regions in global warming and El Niño teleconnections. *Geophysical Research Letters*, *30*(24). https://doi.org/10.1029/2003gl018625

Nicknish, P. A., Chiang, J. C., Hu, A., & Boos, W. R. (2023). Regional tropical rainfall shifts under global warming: An energetic perspective. *Environmental Research: Climate*, *2*(1), 015007. https://doi.org/10.1088/2752-5295/acb9b0

Odoulami, R. C., & Akinsanola, A. (2018). Recent assessment of West African summer monsoon daily rainfall trends. *Weather*, *73*(9), 283–287. https://doi.org/10.1002/wea.2965

Otto-Bliesner, B. L., Brady, E. C., Zhao, A., Brierley, C. M., Axford, Y., Capron, E., et al. (2021). Large-scale features of last interglacial climate: Results from evaluating the lig127k simulations for the Coupled Model Intercomparison Project (CMIP6)–Paleoclimate Modeling Intercomparison Project (PMIP4). *Climate of the Past*, *17*(1), 63–94. https://doi.org/10.5194/cp-17-63-2021

Peng, D., & Zhou, T. (2017). Why was the arid and semiarid northwest China getting wetter in the recent decades? *Journal of Geophysical Research: Atmospheres*, *122*(17), 9060–9075. https://doi.org/10.1002/2016jd026424

Rachmayani, R., Prange, M., & Schulz, M. (2015). North African vegetation–precipitation feedback in early and mid-Holocene climate simulations with CCSM3-DGVM. *Climate of the Past*, *11*(2), 175–185. https://doi.org/10.5194/cp-11-175-2015

Reick, C., Raddatz, T., Brovkin, V., & Gayler, V. (2013). Representation of natural and anthropogenic land cover change in MPI-ESM. *Journal of Advances in Modeling Earth Systems*, *5*(3), 459–482. https://doi.org/10.1002/jame.20022

Reick, C. H., Gayler, V., Goll, D., Hagemann, S., Heidkamp, M., Nabel, J. E., et al. (2021). Jsbach 3-the land component of the MPI earth system model: Documentation of version 3.2.

Rowell, D. P. (2003). The impact of Mediterranean SSTS on the Sahelian rainfall season. *Journal of Climate*, *16*(5), 849–862. https://doi.org/10.1175/1520-0442(2003)016<0849:tiomso>2.0.co;2

Rowell, D. P., Senior, C. A., Vellinga, M., & Graham, R. J. (2016). Can climate projection uncertainty be constrained over Africa using metrics of contemporary performance? *Climatic Change*, *134*(4), 621–633. https://doi.org/10.1007/s10584-015-1554-4

Schneider, T., Bischoff, T., & Haug, G. H. (2014). Migrations and dynamics of the intertropical convergence zone. *Nature*, *513*(7516), 45–53. https://doi.org/10.1038/nature13636

Scussolini, P., Bakker, P., Guo, C., Stepanek, C., Zhang, Q., Braconnot, P., et al. (2019). Agreement between reconstructed and modeled boreal precipitation of the last interglacial. *Science Advances*, *5*(11), eaax7047. https://doi.org/10.1126/sciadv.aax7047

Semmler, T., Danilov, S., Gierz, P., Goessling, H. F., Hegewald, J., Hinrichs, C., et al. (2020). Simulations for CMIP6 with the AWI climate model AWI-CM-1-1. *Journal of Advances in Modeling Earth Systems*, *12*(9), e2019MS002009. https://doi.org/10.1029/2019ms002009

Shi, X. (2024). Doubling CO_2 experiments under various climate states based on AWIESM2 [Dataset]. *Zenodo*. https://doi.org/10.5281/zenodo.11183138

Shi, X., Werner, M., Krug, C., Brierley, C. M., Zhao, A., Igbinosa, E., et al. (2022). Calendar effects on surface air temperature and precipitation based on model-ensemble equilibrium and transient simulations from PMIP4 and PACMEDY. *Climate of the Past*, *18*(5), 1047–1070. https://doi.org/10.5194/cp-18-1047-2022

Shi, X., Werner, M., Wang, Q., Yang, H., & Lohmann, G. (2022). Simulated mid-Holocene and last interglacial climate using two generations of AWI-ESM. *Journal of Climate*, *35*(23), 7811–7831. https://doi.org/10.1175/jcli-d-22-0354.1

Shi, X., Werner, M., Yang, H., D'Agostino, R., Liu, J., Yang, C., & Lohmann, G. (2023). Unraveling the complexities of the last glacial maximum climate: The role of individual boundary conditions and forcings. *Climate of the Past*, *19*(11), 2157–2175.

Sidorenko, D., Goessling, H. F., Koldunov, N., Scholz, P., Danilov, S., Barbi, D., et al. (2019). Evaluation of FESOM2. 0 coupled to ECHAM6. 3: Preindustrial and HIGHResMIP simulations. *Journal of Advances in Modeling Earth Systems*, *11*(11), 3794–3815. https://doi.org/10.1029/2019ms001696

Sidorenko, D., Rackow, T., Jung, T., Semmler, T., Barbi, D., Danilov, S., et al. (2015). Towards multi-resolution global climate modeling with ECHAM6–FESOM. Part I: Model formulation and mean climate. *Climate Dynamics*, *44*(3–4), 757–780. https://doi.org/10.1007/s00382-014-2290-6

Stevens, B., Giorgetta, M., Esch, M., Mauritsen, T., Crueger, T., Rast, S., et al. (2013). Atmospheric component of the MPI-M Earth system model: ECHAM6. *Journal of Advances in Modeling Earth Systems*, *5*(2), 146–172. https://doi.org/10.1002/jame.20015

Stouffer, R. J., Yin, J.-j., Gregory, J., Dixon, K., Spelman, M., Hurlin, W., et al. (2006). Investigating the causes of the response of the thermohaline circulation to past and future climate changes. *Journal of Climate*, *19*(8), 1365–1387. https://doi.org/10.1175/jcli3689.1

Trenberth, K. E., & Guillemot, C. J. (1995). Evaluation of the global atmospheric moisture budget as seen from analyses. *Journal of Climate*, *8*(9), 2255–2272. https://doi.org/10.1175/1520-0442(1995)008<2255:eotgam>2.0.co;2

Walker, J. M. (2017). *Seasonal and interannual variability in South Asian monsoon dynamics*. California Institute of Technology.

Yang, H., Lohmann, G., Lu, J., Gowan, E. J., Shi, X., Liu, J., & Wang, Q. (2020). Tropical expansion driven by poleward advancing midlatitude meridional temperature gradients. *Journal of Geophysical Research: Atmospheres*, *125*(16), e2020JD033158. https://doi.org/10.1029/2020jd033158

Yang, H., Lohmann, G., Shi, X., & Müller, J. (2023). Evaluating the mechanism of tropical expansion using idealized numerical experiments. *Ocean-Land-Atmosphere Research*, *2*, 0004.

References From the Supporting Information

Berger, A. (1977). Long-term variations of the earth's orbital elements. *Celestial Mechanics*, *15*(1), 53–74. https://doi.org/10.1007/bf01229048

Briggs, R. D., Pollard, D., & Tarasov, L. (2014). A data-constrained large ensemble analysis of Antarctic evolution since the EEMIAN. *Quaternary Science Reviews*, *103*, 91–115. https://doi.org/10.1016/j.quascirev.2014.09.003

Buiron, D., Chappellaz, J., Stenni, B., Frezzotti, M., Baumgartner, M., Capron, E., et al. (2011). TALDICE-1 age scale of the Talos Dome deep ice core, East Antarctica. *Climate of the Past*, *7*(1), 1–16. https://doi.org/10.5194/cp-7-1-2011

Flückiger, J., Monnin, E., Stauffer, B., Schwander, J., Stocker, T. F., Chappellaz, J., et al. (2002). High-resolution Holocene N_2O ice core record and its relationship with CH_4 and CO_2. *Global Biogeochemical Cycles*, *16*(1), 10–11. https://doi.org/10.1029/2001gb001417

Köhler, P., Nehrbass-Ahles, C., Schmitt, J., Stocker, T. F., & Fischer, H. (2017). A 156 kyr smoothed history of the atmospheric greenhouse gases CO_2, CH_4, and N_2O and their radiative forcing. *Earth System Science Data*, *9*(1), 363–387. https://doi.org/10.5194/essd-9-363-2017

Levitus, S., Locarnini, R. A., Boyer, T. P., Mishonov, A. V., Antonov, J. I., Garcia, H. E., et al. (2010). World ocean atlas 2009.

Monnin, E., Steig, E. J., Siegenthaler, U., Kawamura, K., Schwander, J., Stauffer, B., et al. (2004). Evidence for substantial accumulation rate variability in Antarctica during the Holocene, through synchronization of CO_2 in the Taylor Dome, Dome C and DML ice cores. *Earth and Planetary Science Letters*, *224*(1–2), 45–54. https://doi.org/10.1016/j.epsl.2004.05.007

Otto-Bliesner, B., Braconnot, P., Harrison, S., Lunt, D., Abe-Ouchi, A., Albani, S., et al. (2017). The PMIP4 contribution to CMIP6–part 2: Two interglacials, scientific objective and experimental design for Holocene and last interglacial simulations. *Geoscientific Model Development*, *10*(11), 3979–4003. https://doi.org/10.5194/gmd-10-3979-2017

Roeckner, E., Brokopf, R., Esch, M., Giorgetta, M., Hagemann, S., Kornblueh, L., et al. (2004). *The atmospheric general circulation model ECHAM5 part Ii: Sensitivity of simulated climate to horizontal and vertical resolution. Report*. Max-Planck-Institut für Meteorologie, 354.

Schilt, A., Baumgartner, M., Blunier, T., Schwander, J., Spahni, R., Fischer, H., & Stocker, T. F. (2010). Glacial–interglacial and millennial-scale variations in the atmospheric nitrous oxide concentration during the last 800,000 years. *Quaternary Science Reviews*, *29*(1–2), 182–192. https://doi.org/10.1016/j.quascirev.2009.03.011

Schneider, R., Schmitt, J., Köhler, P., Joos, F., & Fischer, H. (2013). A reconstruction of atmospheric carbon dioxide and its stable carbon isotopic composition from the penultimate glacial maximum to the last glacial inception. *Climate of the Past*, *9*(6), 2507–2523. https://doi.org/10.5194/cp-9-2507-2013

Tarasov, L., Dyke, A. S., Neal, R. M., & Peltier, W. R. (2012). A data-calibrated distribution of deglacial chronologies for the North American ice complex from glaciological modeling. *Earth and Planetary Science Letters*, *315*, 30–40. https://doi.org/10.1016/j.epsl.2011.09.010

Tarasov, L., & Peltier, W. R. (2003). Greenland glacial history, borehole constraints, and EEMIAN extent. *Journal of Geophysical Research*, *108*(B3). https://doi.org/10.1029/2001jb001731

Werner, M., Haese, B., Xu, X., Zhang, X., Butzin, M., & Lohmann, G. (2016). Glacial–interglacial changes in $H_2^{18}O$, HDO and deuterium excess–results from the fully coupled ECHAM5/MPI-OM Earth system model. *Geoscientific Model Development*, *9*(2), 647–670. https://doi.org/10.5194/gmd-9-647-2016